RAPID PROTOTYPING AND TESTING OF A SMALL SCALE FAN FOR CSP POWER PLANT APPLICATIONS

David VOLPONI[1], Tommaso BONANNI[1], Gino ANGELINI[1], Lorenzo TIEGHI[1], Giovanni DELIBRA[1], Alessandro CORSINI[1], Michael WILKINSON[2], Sybrand VAN DER SPUY[2], Theodor W. VON BACKSTRÖM[2]

1 Sapienza University of Rome, Dept. of Mechanical and Aerospace Engineering, Via Eudossiana 18, 00184 Roma, Italy

[2] Stellenbosch University, Department of Mechanical and Mechatronic Engineering, Joubert Street, Stellenbosch, 7600, South Africa

SUMMARY

A 7.3152 m. diameter axial flow fan was developed in a previous study for a hybrid cooling application, specifically aimed at concentrated solar power (CSP) plants. In order to assess the performance of this fan in sufficient detail a 630 mm diameter scale model is manufactured by means of rapid prototyping. The performance of this fan is subsequently compared to the simulated and experimental results of a 1.5 m diameter fan of the same design.

INTRODUCTION

The MinWaterCSP project aims to reduce the cooling water consumption of concentrating solar power (CSP) plants and improve plant efficiency through the introduction of novel dry/wet cooling technology [1]. Although the use of dry-cooling holds advantages in terms of water consumption for CSP plants that are typically located in arid regions, they also have disadvantages in terms of heat transfer performance. Dry cooled condensers are typically mounted well above ground level, where fans mounted below condenser bundles drive air upwards, allowing heat transfer to take place. The performance of these systems can be adversely affected by high ambient temperatures or wind effects which subject the fans to distorted inflow conditions, reducing fan performance and thereby the overall heat transfer performance of the heat exchanger. The MinWaterCSP projects aims to reduce this effect by introducing a hybrid cooler into the cooling circuit, which can boost heat transfer performance when the plant is exposed to extreme ambient conditions.

As part of the project a new axial flow fan was developed and manufactured for a 7.3152 m, full scale test facility, located at Stellenbosch University built within the framework of the MinWaterCSP project. This fan is referred to as the M-fan. The M-fan was designed to meet the requirements of a high design flow rate (333 m^3/s) and low pressure rise (116.7 Pa), typically

associated with large diameter cooling fans [2]. The design objectives had to be met at a maximised operating point fan total-to-static efficiency. The design procedure followed is loosely based on the work of Bruneau [2] and van der Spuy et al [3] and it is described in detail by Wilkinson et al [4].

To confirm the design of the M-fan, a 1.5 m diameter prototype was manufactured and its performance was measured in a 1.5 m diameter ISO 5801, Type A fan test facility [5]. This was followed by the rapid prototype manufacture and testing of a 630 mm diameter model of the M-fan in a 630 mm ducted fan test facility, also at Stellenbosch University. Fan characteristic tests as well as flow field measurements upstream and downstream of the fan rotor are performed on the 630 mm fan.

DEVELOPMENT OF THE M-FAN

As mentioned previously, the fan presented in this study is referred to as the M-Fan and is depicted in Figure 1. The M-Fan is the result of a design procedure conceived to produce not only an efficient axial flow fan but also one that can perform well when subjected to off design conditions commonly encountered in air-cooled heat exchangers.

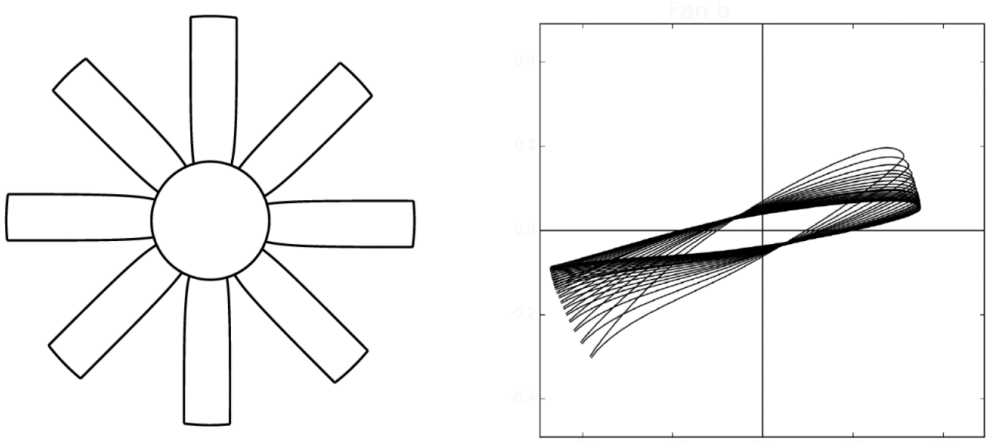

Figure 1- Schematic of the M-fan (Left) and Stacking profile (Right) [4]

The design objective was achieved by means of several optimisation steps (listed in the block diagram reported in Figure 2) including: (i) selection of the hub-tip ratio, (ii) vortex distribution, (iii) blading and aerofoil camber distributions in order to attain maximised total-to-static efficiency at the design point and a pressure characteristic which strongly decreases from full load to no load.

All optimisation steps were conducted independently from one another. This was done intentionally, to check the validity of each calculation step. The design procedure is implemented by means of a PYTHON [5] script with XFOIL [6] being used for aerofoil camber adjustment and polar prediction and Vanderplaats Research and Development DOT software [7] which provides a suite of numerical optimisation tools. The final output of the PYTHON script is a text file containing key parameters such as rotor outlet flow distribution, chord and blade twist distributions as well as coordinate files that are used to define the blade in a CAD program.

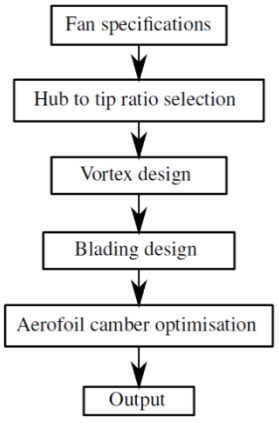

Figure 2- Design Procedure (adapted from [4])

Key physical parameters and performance estimates for the M-Fan are shown in Table 1.

Table 1 – M-Fan full scale characteristics

Diameter	7.3152 m
Number of blades	8
Hub To Tip Ratio	0.29
Maximum Tip Gap	30 mm
Fan Rotational Speed	151 RPM
Flow Rate	333 m^3/s
Estimated Fan Total-to-Static Pressure	116.7 Pa
Estimated Fan Shaft Power	63285.21 W
Estimated Fan Total-to-Static Efficiency	61.4 %

The fan has an aerofoil camber distribution of 3.5% at the hub and 0.8 % at the blade tip, the aerofoil sections used are camber modified versions of the NASA LS 413 section. The blades have an almost rectangular shape and do not taper much between the hub and tip, as can be seen in Figure 1. This is due to a set of constraints imposed by the fan manufacturing company including limiting the maximum chord length at the hub to 1 m, combined with a constraint requiring a linear chord distribution. These design features do however have the benefit of increasing the Reynolds numbers near the blade tip, reducing drag and improving fan total-to-static efficiency.

The root blade angle is 34 degrees and the angle of attack at the blade root is 2.8 degrees at the design point. This should give the fan a reasonable stall tolerance at low flow rates, as stall tends to occur at an angle of attack of approximately 14 degrees for the aerofoil sections used. It should also be noted that the blade tip speed is 58 m/s, the maximum allowed by the design specifications. Lower speeds result in reduced total-to-static efficiency, due to lower Reynolds numbers and increased blade angles.

NUMERICAL MODELLING OF THE M-FAN

Once blade geometry and rotor configuration were defined, the performance of the design was verified using computational fluid dynamics (CFD) tools. A periodic three dimensional model of a single blade passage similar to that of Louw [8] was developed and the simulations were run using ANSYS FLUENT 17.2.

The periodic three dimensional model includes a single blade passage with periodic boundary conditions along the symmetry planes of the fan. For the purposes of this study the blade was run with zero tip clearance, as the design code does not account for tip gap effects. Three dimensional modelling of turbomachinery is computationally expensive and periodic three dimensional modelling provides a means to reduce computational load compared to modelling all eight blades in a rotating domain. The computational domain and boundary conditions are shown in Figure *3*.

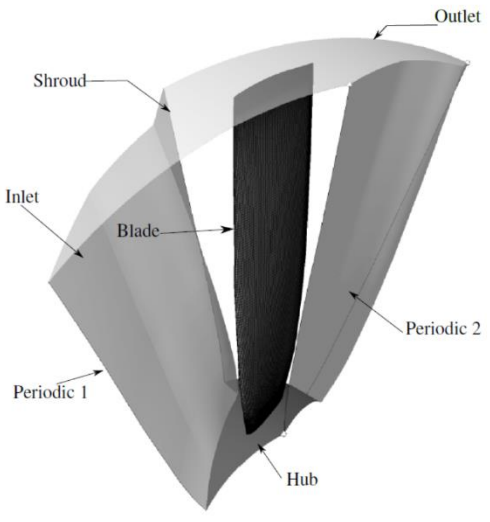

Figure 3 - Periodic three dimensional domain [4]

The inlet boundary condition was set to be a massflow inlet. Stationary wall boundary conditions were applied at the blade and hub surfaces whereas the shroud was set to be a rotating wall in order to be stationary relative to the rotating domain. The outlet was set to be a pressure outlet with a gauge pressure of 0 Pa. The entire domain was specified to rotate at the fan rotational speed in order to represent a rotating blade.

The realizable k-ε turbulence model was used with enhanced wall functions. Values of y+ were between 0 and 300, which is considered acceptable for this approach. Turbulence intensity at the inlet was set to 3 % at the inlet with a viscosity ratio of 0.01. Additional solver setting are presented in Table 2.

Table 2 - CFD Solver settings

Pressure-Velocity Coupling	SIMPLE
Pressure	PRESTO!
Gradient	Least Squares Cell Based
Momentum	QUICK
Turbulent Kinetic Energy	QUICK
Turbulent Dissipation Rate	QUICK

In order to obtain convergence the model was first run with first order momentum and turbulence settings before being switched to the higher order schemes as the simulation neared convergence. Final convergence levels obtained were in the order of 10^{-4}.

Simulations were performed at six different flow rates in order to obtain a prediction of the performance across the normal operating range of the M-Fan. The fan total-to-static efficiency, total-to-static pressure and absorbed power characteristics are depicted in Figure 4 and Figure 5.

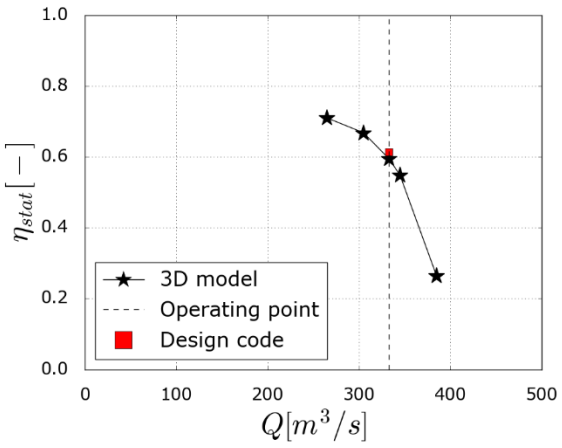

Figure 4 – M-Fan total to static efficiency η_{stat}

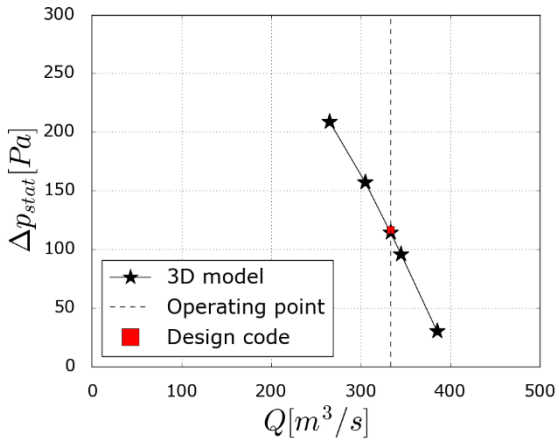

Figure 5 – M-Fan total to static pressure rise Δp_{stat}

The numerical results show good agreement with the design code estimated total-to-static pressure at the design point. It is also noted that the 3D model predicts a steep total-to-static pressure characteristic at reduced flow rates. This is important as it has been shown that fans with steep pressure characteristics are better suited to air-cooled heat exchanger applications where distorted inflows are encountered [2]. A fan with a steep total-to-static pressure characteristic will not deviate as far from the design flow rate as a fan with a shallower pressure characteristic. This is due to the increase in pressure required to overcome the distorted inflow resulting in a smaller reduction in flow rate, and therefore heat transfer performance. These results indicate that the fan is suitable for its given application.

The discrepancy between the design and computed values in terms of total-to-static efficiency and total-to-static pressure are reported in Table 3. The error between the 3D model and the design code indicates that the design assumptions made are reasonable and have little effect on the fan achieving the desired total-to-static pressure rise. In terms of efficiency 1% of the error between the 3D model and design code can be ascribed in part to the pressure discrepancy, and the remaining error is due to the higher power predicted by the 3D model.

Table 3 - Comparison of performance characteristics

	Design Code	CFD
Fan Static Pressure	116.7 Pa	114.7 Pa
Fan Static Efficiency	61.4 %	59.4 %
Fan Power	63285.2 W	64241.1 W

EXPERIMENTAL EVALUATION OF THE 1.5 m M-FAN

A 1.542 m (shroud) diameter model of M-Fan was built and tested to obtain its characteristic curves and confirm the design and numerical modelling verification processes. Measurements were conducted in a test facility that complies with the ISO 5801:2007 Part 1 requirements [5]. During a typical fan test, flow is drawn into the facility through a calibrated bellmouth inlet at location 1 (Figure *6*). The flow through the facility is controlled by a set of louvers (2), downstream of which flow straighteners order the flow and reduce turbulence. An auxiliary fan located at section 3 is used to overcome the pressure losses resulting from the flow straighteners and louvers at higher flow rates. The flow then passes through a second set of straighteners in order to remove any swirl and is expanded into the settling chamber. A set of guide vanes (4) at the inlet of the settling chamber ensure even flow distribution. A set of three wire screens in the middle of the settling chamber (5) conditions the flow as it enters into the final part of the settling chamber (6). From here, flow is finally drawn out to the atmosphere through the test fan (7).
During a single characteristic test run, measurements are taken at a range of flow rates. These measurements include:

- Static pressure difference ($\Delta p_{s,\ bell}$) relative to atmospheric pressure at the calibrated bellmouth inlet.
- Static pressure difference ($\Delta p_{s,\ plen}$) relative to atmospheric pressure inside the plenum chamber.
- Shaft rotational speed (ω).
- Shaft torque (τ).

Additional measurements include the air temperature (T_a) inside the test facility and the barometric pressure (p_{atm}). These measurements are only made once before and after each test run and are averaged in order to calculate the mean air density (ρ_a) over the course of the test run. The accuracy of quantities measured during the tests is reported in Table 4. Uncertainty on the blade angle setting of each blade was less than 0.28 degrees. Experimental results for the M-Fan operating with a 34 degree blade angle are depicted in Figure 7 and Figure 8.

Table 4 - Uncertainties on measured quantities during a single measurement for 1.5 m test facility

Quantity	Maximum std. deviation	Unit	% error
Inlet pressure	2.551	Pa	1.38

Plenum pressure	2.630	Pa	1.45
Shaft torque	0.280	Nm	0.806
Shaft rotational speed	0.262	RPM	0.036
Volume flow rate	0.08	m^3/s	0.607

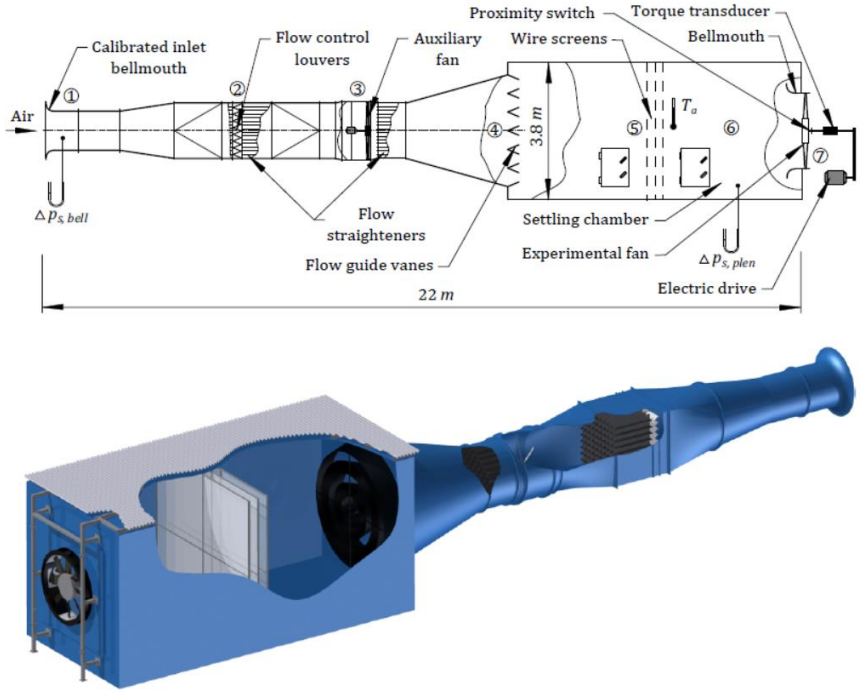

Figure 6 – The ISO 5801 test facility at Stellenbosch University, sketch (top) and isometric view (bottom) [8]

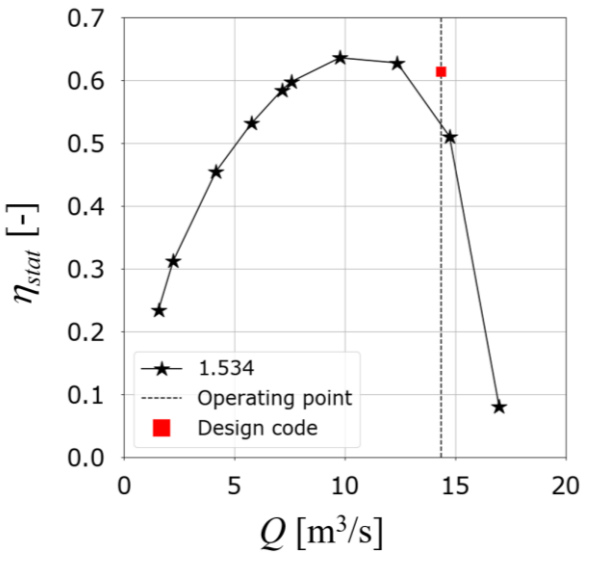

Figure 7 - 1.5m M-Fan total-to-static efficiency (η_{stat})

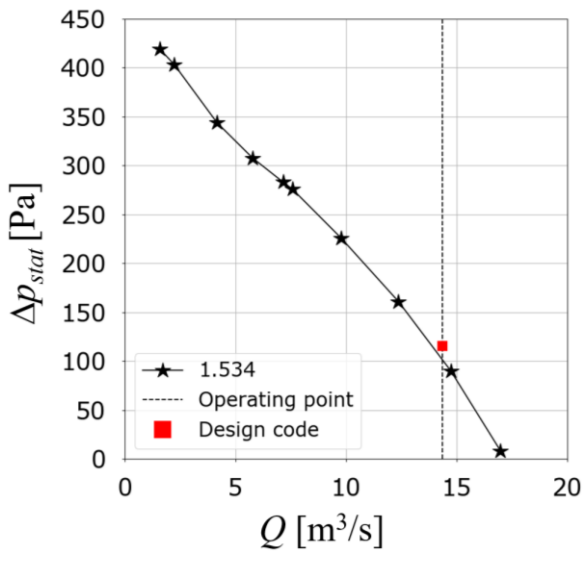

Figure 8 - 1.5m M-Fan total-to-static pressure rise (Δp_{stat})

EXPERIMENTAL EVALUATION OF THE 0.63 m M-FAN

A 630 mm (shroud) diameter model of the M-Fan was built in order to investigate the velocity distributions upstream and downstream of the test fan. The fan dimensions and operating conditions

are scaled using the fan affinity laws. Although dynamic similarity could not be attained (dissimilar Reynolds number values) kinematic and geometric similarity were applied. The fan blades were printed by means of a commercially available, medium-to-low quality, 3D printer.

The height of each print was limited to fit the capability of the printer, in this case 140 mm, and so a single blade was printed in two separated parts. The root of the 3D printed fan blade is designed with a means to set the blades at three different b angles. In order to simplify the final blade assembly, reference holes were printed directly in the final geometry as shown in 9. A differential infill was used for the two parts, the hub part, which was expected to be the most mechanically stressed, uses a 100% infill, while for the tip part the infill was 25 %. This guaranteed a consistent weight reduction and adequate blade stiffness. The two blade parts were assembled by means of two wooden dowel pins and glue providing excellent surface continuity between the two adjacent parts. In order to assess the precision of the final blade, the blade twist was measured, with the maximum error in twist being below 0.25 degrees, both in hub and tip regions.

One issue that was noted with the manufacture of the 3D printed blade was the inability of the machine to print the fine trailing edge of the blades that resulted from the geometric scaling. To compensate for this, the manufacturer produced the blades with a chord length that is 5 mm shorter than intended, as the trailing edge would otherwise be thinner than the printer nozzle (< 0.4 mm).

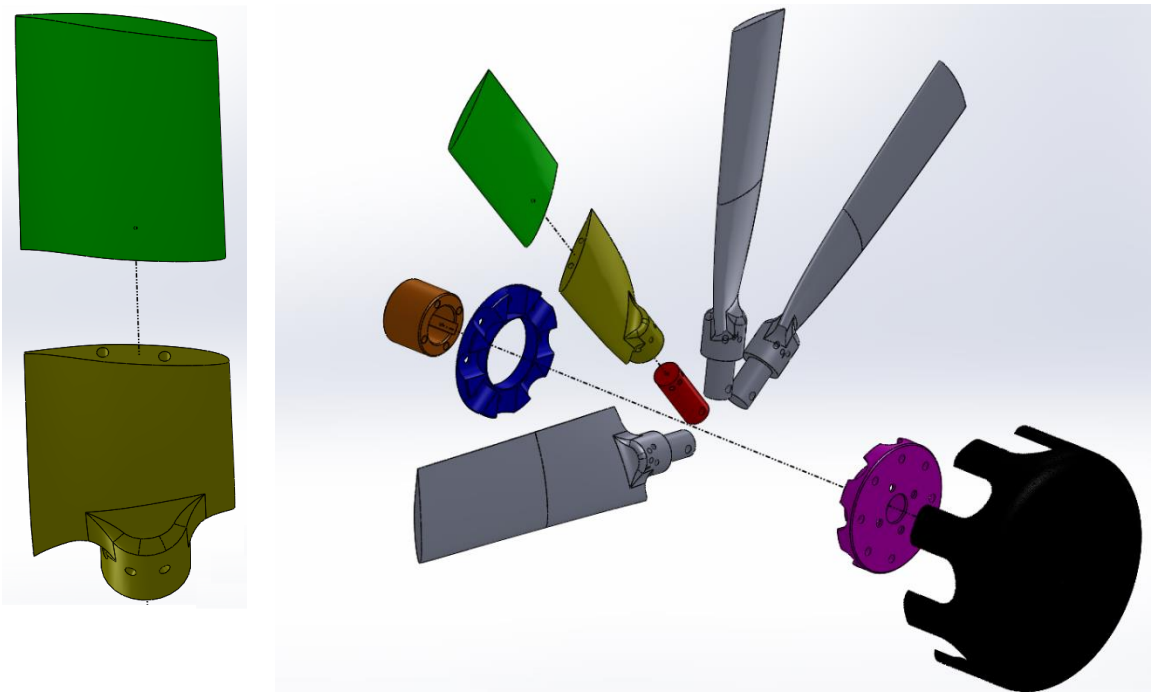

Figure 9 - Final Blade geometry (Left) and half-impeller assembly (Right)

Measurements were conducted in an experimental facility that is compliant with ISO 5801:2007, Type D, with same procedure described before. A sketch of the test rig is shown in

Figure 10.

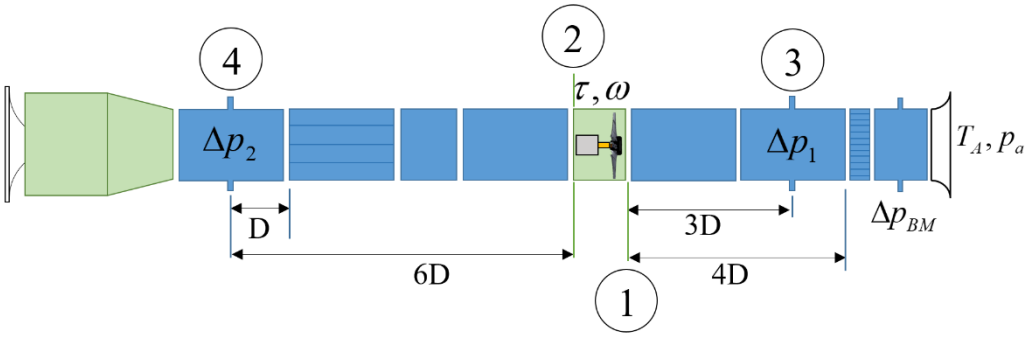

Figure 10 – The 630 mm test facility at Stellenbosch University

To ensure the same tip speed of 58 m/s, the fan was run at 1769 rpm. The target fan total-to-static pressure was 116.7 at 2.44 m^3/s. Table 5 reports interpolated performance at the duty point .The performance characteristic of the 630 mm fan are reported in

Figure 11 for different blade angles.

Table 5 - Interpolated Performance at the duty point for the 630 mm M-Fan

M-Fan 630mm	
Fan Static Pressure	116.7 Pa
Fan Static Efficiency	49.32 %
Fan Absorbed Power	577.34 W
Blade angle	35.4

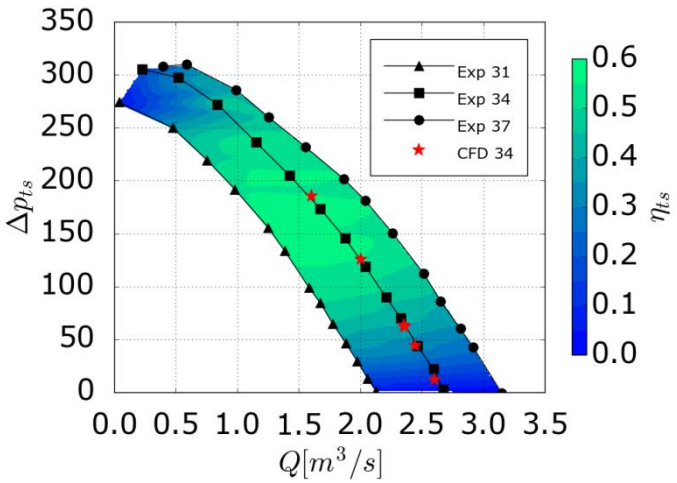

Figure 11 – 630 mm M-Fan fan static pressure rise and efficiency contours for different blade angles

The reduced model dimensions allow the velocity components and pressures upstream and downstream of the fan to be measured using a five-hole pneumatic pressure probe (see Figure 12). These measurements are used to calculate the velocity distributions downstream the fan and compare the results to the design values. Additionally a 3D RANS CFD model of the 630 mm fan has been developed and validated against the fan performance characteristics, as shown in Figure 11. The model consists of a one eighth segment of the test facility shown in Figure 10, which is assumed to be rotationally periodic. The model is developed in a similar manner to the 24 ft fan model and is also simulated in ANSYS 17.2, however the model includes the fan hub rather than simplifying the geometry to an annulus. Geometric simplifications include replacing the inlet bellmouth with a mass flow inlet boundary condition as well as placing the outlet boundary before

the star straightener. The fan is modelled with a 2 mm tip clearance in order to be identical to the experimental case. The realizable k-ε model is used for turbulence closure. The flow fields predicted by this model will be compared to the flow fields measured by the five-hole probe, in order to ascertain the CFD model's ability to predict the flow field downstream of the fan.

HOLE PROBE CALIBRATION AND RESULTS

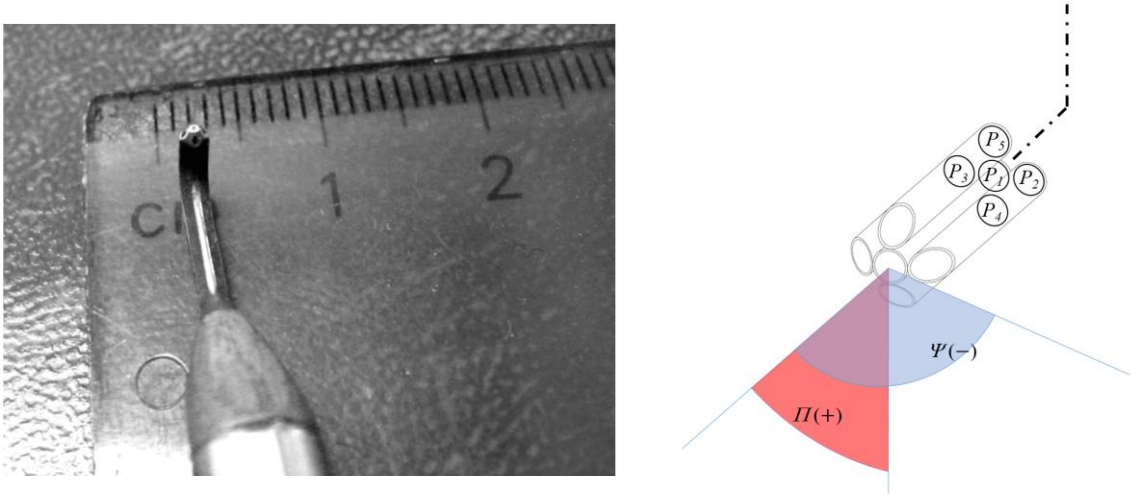

Figure 12 - Five holes probe picture shown next to a cm scale (Left) and schematic (Right)

The five-hole probe is calibrated in a low speed wind tunnel. A variable speed drive is used to regulate the wind tunnel fan, which was set to have a test section velocity of 8.5 m/s. Time averaged measurements of different pressure coefficients [9], that account for differences of pressures between different holes in the probe are calculated and stored in a test matrices for different pitch (Π) and yaw (Ψ) angles (see Figure 12).

The coefficients are calculated using the following equations:

$$\bar{P} = \frac{P_2 + P_3 + P_4 + P_5}{4} \quad (1)$$

$$Cp_{centre} = \frac{P_1 - P_{stat}}{P_{tot} - P_{stat}} \quad (2)$$

$$Cp_{average} = \frac{\bar{P} - P_{stat}}{P_{tot} - P_{stat}} \quad (3)$$

$$Cp_{\Psi} = \frac{P_2 - P_3}{P_1 - \bar{P}} \quad (4)$$

$$Cp_{\Pi} = \frac{P_4 - P_5}{P_1 - \bar{P}} \quad (5)$$

Figure 13 and Figure 14 illustrate the calibration maps of the centre and average pressure coefficients. These figures show that the probe is quite symmetrical on the yaw and pitch axes.

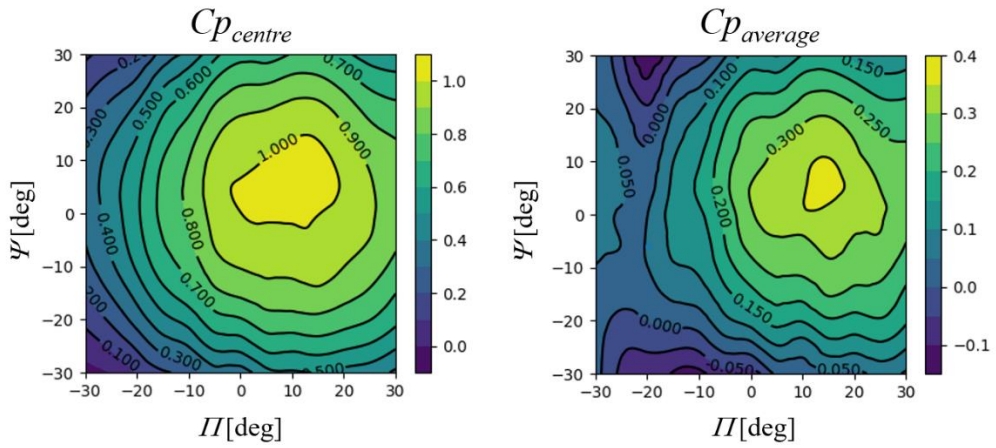

Figure 13 - Cp_{centre} (Left) and $Cp_{average}$ (Right) calibration maps

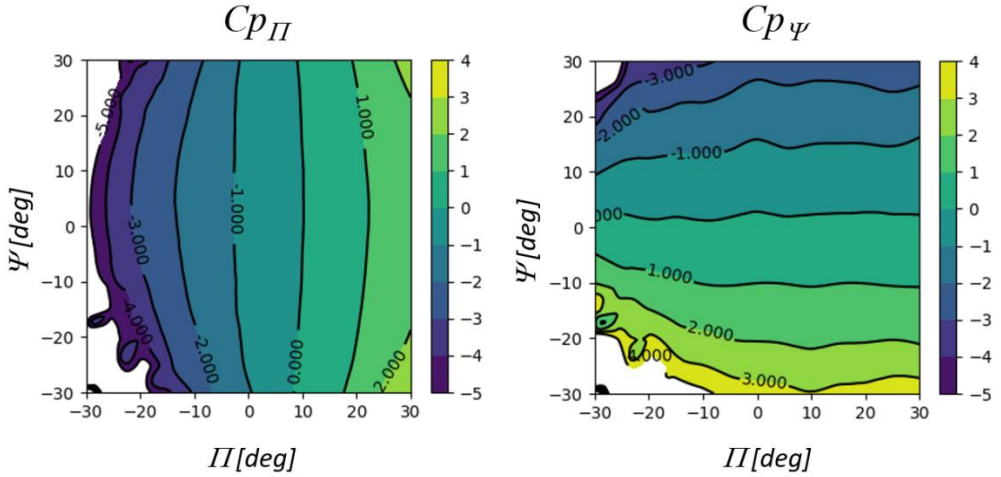

Figure 14 – Cp_{Π} (left) and Cp_{Ψ} (right) Calibration Maps

The pitch and yaw angles can be determined by combining the pitch and yaw calibration maps. This is achieved, as described by Kirstein [10], by using the pitch and yaw coefficients, and then superimposing their intersections with corresponding maps.

Once the yaw and pitch angles are known, the Cp_{centre} and $Cp_{average}$ values can be obtained and converted to total and static pressures. To convert the coefficients to static and total pressure equations 1 to 5 are rearranged to get:

$$P_{stat} = \frac{Cp_{centre}.\bar{P} - Cp_{average}.P_1}{Cp_{centre} - Cp_{average}} \quad (6)$$

$$P_{tot} = P_{stat} + \frac{P_1 - P_{stat}}{Cp_{centre}} \quad (7)$$

Once the angles and dynamic pressure are found, the velocities can be calculated using Bernoulli's principle. After an error estimation based on variance analysis an uncertainty of 1° must be considered for the yaw angles and 2° for the pitch angles.

FLOW FIELD ANALYSIS

A comparison between circumferentially averaged velocity fields at the blade outlet plane of both experimental five holes probe and CFD are compared to the profiles generated by the design code. Five hole probe measurements are taken five chord lengths downstream of the fan rotor. The CFD data is also extracted 5 chord lengths downstream of the rotor whereas the design data describes the flow field at the immediate exit of the fan. Data presented is referred to a flow of 2.452 m^3/s. The respective axial and tangential velocity profiles are shown in Figures 14 and 15.

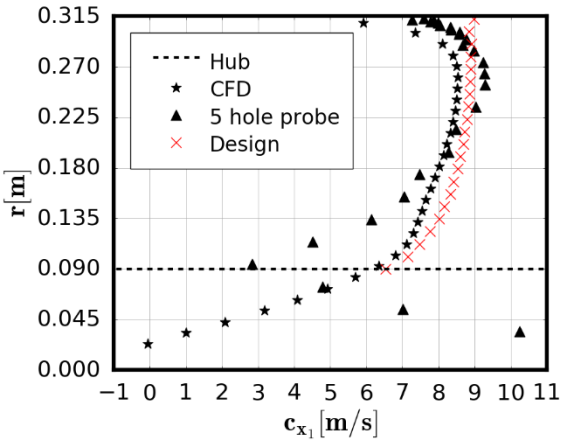

Figure 15 – Axial velocity profiles downstream of fan rotor

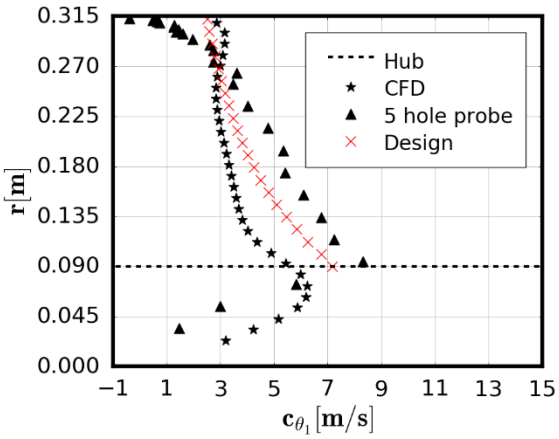

Figure 16 – Tangential velocity profiles downstream of fan rotor

It can be see that the axial velocity profile predicted by the 3D CFD model correlates reasonably with the designed profile at the measurement plane, with some discrepancies occurring due to the flow expanding downstream of the fan annulus (Figure 15). In terms of axial velocity there is also some discrepancy between the CFD and design profiles at the duct, likely due to wall effects between the fan exit and measurement planes. In terms of axial velocity there is some agreement between the 5 hole probe and CFD data near the blade tip, however nearer the hub the 5 hole probe indicates a much lower axial velocity than the CFD or design data. Below the hub radius there is no agreement between the 5 hole probe and CFD data, the reason for this is not clear at this stage.

In terms of tangential velocity the five hole probe data is shown to correlate well with the designed vortex for the majority of the blade span, as shown in Figure 16. It is noted that the tangential velocity component in the measured flow field is greater than that of the design and CFD data. The CFD predicts a smaller tangential velocity over the majority of the blade span. However the measured tangential velocity at the blade tip is lower than both the CFD and design data, likely as a result of wall effects. This may also explain the increase tangential velocity nearer the hub. Below the hub there is little to no correlation between the experimental and numerical data. This result poses several questions as the CFD model has been validated in terms of fan performance characteristics, as shown in Figure 11, indicating that the amount of swirl introduced into the flow in the CFD model is correct. Further investigations into this effect need to be carried out.

CONCLUSIONS

Validation of the design methodology described for a large diameter axial flow fan, previously validated by means of a three dimensional CFD models, is extended with experimental data from two different ISO 5801 standard facilities able to measure fan sizes of respectively 1.542 m and 0.630 m diameter. The methodology is shown to be capable of designing a fan to meet given physical specifications. The design assumptions have been shown to be reasonable in the context of

the flow field in the vicinity of the fan blades as well as in terms of fan performance. The M-Fan is also indicated to be suited to its application in large air-cooled heat exchangers.

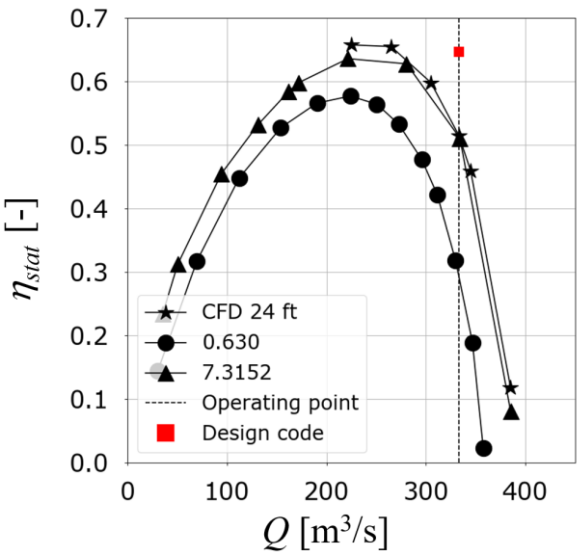

Figure 17 – Different MFan prototypes η_{stat}

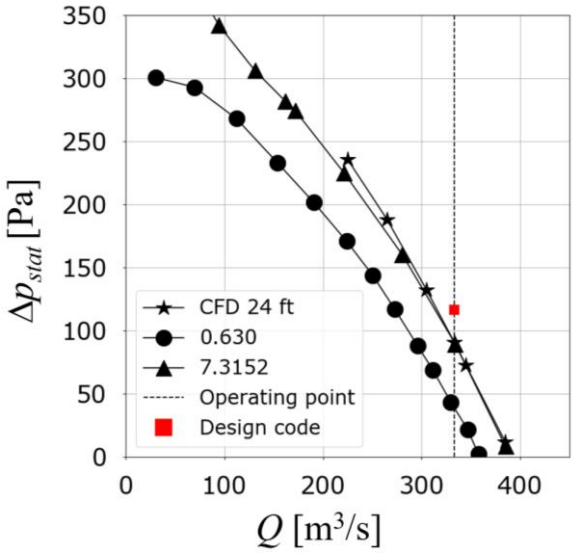

Figure 18 - Different MFan prototypes Δp_{stat}

In Figure 17 and Figure 18 and are reported all data from CFD, and the two different facilities scaled to 24ft dimensions. The correlation between the 1.5 m experimental data and CFD results is seen to be acceptable and small discrepancies can be ascribed to small geometric differences and different installation environments.

Great discrepancies were found between the small scale fan and the CFD in terms of flow field. At this stage the reason for this is not entirely known, however further investigations are planned, including taking flow field measurements nearer the rotor exit as well as at the fan inlet. These investigations aim to understand the influence of inflow conditions on the flow field downstream of the fan as well as providing a better comparison with the design data.

In all conditions the duty point seems to be missed by the 630 mm fan. This is ascribed to the inability of the 3D printer to print the fine trailing edge of the blades that resulted from the geometric scaling. This aspect could dramatically influence the flow turning capability of the blade sections affecting the rotor efficiency. The construction of a geometrically correct 630 mm M-Fan is planned in order to investigate this effect.

ACKNOWLEDGEMENTS

The financial assistance of the National Research Foundation (NRF) towards this research is hereby acknowledged. Opinions expressed and conclusions arrived at, are those of the author and are not necessarily to be attributed to the NRF.

Computations were performed using the University of Stellenbosch's Rhasatsha HPC: http://www.sun.ac.za/hpc.

This project has received funding from the European Union's Horizon 2020 research and innovation programme under grant agreement No. 654443

This communication related to the action MinWaterCSP is made by the beneficiaries and it reflects only the author's view. The European Commission is not responsible for any use that may be made of the information it contains.

BIBLIOGRAPHY

[1] The MinWaterCSP Project - http://www.minwatercsp.eu/minwatercsp_project/ **2017**

[2] Bruneau, P. R. P. – *The design of a single rotor axial flow fan for a cooling tower application*. M Eng. Thesis. Stellenbosch University. **1994**

[3] van der Spuy, S. J., von Backström, T.W. – *Performance of rotor-only axial fans designed for minimum exit kinetic energy*. R&D Journal, Volume 18 (3). **2002**

[4] Wilkinson, M.B., van der Spuy, S. J., von Backström, T.W. – *The Design of a Large Diameter Axial Flow Fan for Air-Cooled Heat Exchanger Applications*. ASME Turbo Expo 2017: Turbomachinery Technical Conference and Exposition. American Society of Mechanical Engineers, p. V001T09A002-V001T09A002. **2017**

[5] ISO 5801: 2007 – *Industrial Fan – Performance Testing using Standardised Airways.* **2007**

[6] van Rossum, G., Drake, F.L. - *The Python Language Reference Manual.* Network Theory Ltd. **2011**

[7] Drela, M. - *Xfoil: An analysis and design system for low Reynolds number airfoils.* Low Reynolds number aerodynamics, pp. 1_12. **1989**

[7] Vanderplaats, G.N. - *Development of a Flexible Optimization Capability.* Vanderplaats R&D Inc, Colorado Springs, Colorado, USA. **1999**

[8] Louw, F.G. – *Investigation of the Flow Field in the Vicinity of an Axial Flow Fan during Low Flow Rates.* PhD. Thesis, Stellenbosch University. **2015**

[9] Ströhmaier, C.K. – *An Evaluation of a Scale Model Medium Speed Wind Tunnel.* M Eng. Thesis, Stellenbosch University. **1996**

[10] Kirstein, C.F., von Backström, T.W. – *Flow through a solar chimney power plant collector-to-chimney transition section.* Journal of Solar Energy Engineering, 128.3: 312-317. **2006**